Finite Element Refinements for Inverse Electrocardiography: Hybrid Shaped Elements and High-Order Element Truncation

DF Wang, RM Kirby, CR Johnson

Scientific Computing and Imaging Institute, University of Utah, Salt Lake City, UT, USA

Abstract

We study how finite element method (FEM) can be selected to optimize numerical discretization of the inverse electrocardiographic (ECG) problem. Due to its ill-posedness, the inverse ECG problem poses different discretization requirements from its forward problem counterpart. Conventional refinements effective for the forward problem may become ineffective when applied to the inverse problem. We propose two refining methods specifically tackling the ill-posedness of the inverse problem. One is hybrid-shaped elements involving quadrilateral/triangular elements in 2D and prismatic/tetrahedral elements in 3D. Another method uses high-order FEM, extracts from the resulting system the linear component and solves the linear part only. Simulations on realistic human torso models demonstrate that both methods improve both the discrete problem's conditioning and the inverse solution, indicating our strategies might provide guidelines for mesh generation in practical biomedical simulations.

1. Introduction

The inverse electrocardiographic (ECG) problem of recovering epicardial potentials from body-surface measurements has wide applications from noninvasive diagnosis of cardiac diseases (*e.g.* ischemia) to guidance of intervention (*e.g.* ablation and defibrillation). ECG simulations include mathematical modeling of the biophysical process and geometric approximation of the anatomical structure of human bodies. We consider the problem that models the cardiac source by epicardial potential distribution, given by:

$$\begin{aligned} \nabla \cdot (\sigma(\boldsymbol{x}) \nabla u(\boldsymbol{x})) &= 0, \quad \boldsymbol{x} \in \Omega && (1) \\ u(\boldsymbol{x}) &= u_0(\boldsymbol{x}), \ \boldsymbol{x} \in \Gamma_H && (2) \\ \vec{n} \cdot \sigma(\boldsymbol{x}) \nabla u(\boldsymbol{x}) &= 0, \quad \boldsymbol{x} \in \Gamma_T, && (3) \\ u(\boldsymbol{x}) &= g(\boldsymbol{x}), \ \boldsymbol{x} \in \Gamma_T, && (4) \end{aligned}$$

Email: {dfwang,kirby,crj}@sci.utah.edu. This work was funded by NSF Career Award (Kirby) NSF-CCF0347791 and NIH NCRR Grant No. 5P41RR012553-10.

where Ω is the torso volume bounded by the epicardium Γ_H and the torso surface Γ_T. $u(\boldsymbol{x})$ is the potential field on Ω, u_0 is the epicardial potential, and g denotes the measured body-surface potential. σ is the conductivity tensor and $\vec{n}$ denotes the outward facing vector normal to Γ_T. The forward problem seeks the potential field $u(\boldsymbol{x})$ given the cardiac source u_0. The inverse problem attempts to recover u_0 from the measurement g.

This paper studies discretization strategies when the governing equations are solved by the finite element methods (FEM). While most refinement methods are able to achieve satisfactory accuracy for the forward problem, the ill-posedness of the inverse problem requires different refinement considerations than its forward counterpart[1]. After showing that the conditioning property of the numerical system is subject to how the FEM is applied and refined, we propose two methods that specifically tackle the concerns of the inverse problem: (1) hybrid finite elements and (2) linear component truncation from high-order elements. Both methods alleviate the ill-conditioning of the numerical system to be solved, and both can be combined with other classical regularization methods to further improve the inverse solution accuracy.

2. Discretization and refinement

Finite Element Discretization. In a theoretical FEM approach, the potential field $u(\boldsymbol{x})$ can be decomposed into $u(\boldsymbol{x}) = v(\boldsymbol{x}) + w(\boldsymbol{x})$ where $w(\boldsymbol{x})$ satisfies boundary conditions (2) and (3) and $v(\boldsymbol{x})$ is a homogeneous term characterized by:

$$\begin{aligned} \nabla \cdot (\sigma \nabla v(\boldsymbol{x})) &= -\nabla \cdot (\sigma \nabla w(\boldsymbol{x})), \ \boldsymbol{x} \in \Omega && (5) \\ v(\boldsymbol{x}) &= 0, \quad \boldsymbol{x} \in \Gamma_D && (6) \\ \vec{n} \cdot \sigma \nabla v(\boldsymbol{x}) &= 0, \quad \boldsymbol{x} \in \Gamma_N && (7) \end{aligned}$$

Here, one first projects the source term from the epicardium onto the function space over the entire domain (by setting $\boldsymbol{w}$), then solves a homogeneous problem whose forcing function is the source after projection. This formulation reveals three approximation issues: 1) the accuracy of the epicardial potential $u_0(\boldsymbol{x})$, 2) the accuracy of the

projection operator $\boldsymbol{w}$, and 3) the accuracy of solving the homogeneous problem $v(\boldsymbol{x})$.

A practical finite element application tessellates Ω and constructs a set of basis functions $\{\phi_i\}$, each of which is associated with one node. The potential field $u(\boldsymbol{x})$ is approximated by the linear combination of the basis functions. The coefficient of each basis function is the potential value at its associated node. Substituting this expansion into (1) and applying the Galerkin method yield a linear system of the form:

$$\begin{pmatrix} \mathbf{A}_{II} & \mathbf{A}_{IT} \\ \mathbf{A}_{TI} & \mathbf{A}_{TT} \end{pmatrix} \begin{pmatrix} \mathbf{u}_I \\ \mathbf{u}_T \end{pmatrix} = \begin{pmatrix} -\mathbf{A}_{IH} \\ 0 \end{pmatrix} \mathbf{u}_H \quad (8)$$

where $\mathbf{u}_H$, $\mathbf{u}_T$, and $\mathbf{u}_I$ denote the vector of potentials on the discretized heart surface(H), torso surface(T), and interior volume(I). The stiffness matrix A is given by $A_{i,j} = \int_\Omega \nabla\phi_i \nabla\phi_j$. A is partitioned based on the three divisions H,I, and T. Its capitalized subscript in (8) shows the interaction between each two divisions.

From (8) we derive the relation between $\boldsymbol{u}_H$ and $\boldsymbol{u}_T$:

$$\mathbf{u}_T = \mathbf{K}\mathbf{u}_H \quad (9)$$

where $\mathbf{K}$ is named the transfer matrix and severely ill-conditioned. The inverse ECG problem intends to solve (9). Note that (8) is a special case of the general approach given by (5): the projection $\boldsymbol{w}$ is set piecewise-linear in the first layer of elements adjacent to the heart surface and zero elsewhere. (8) hence exemplifies the aforementioned three issues. Once the resolution of $\mathbf{u}_H$ is determined, the accuracy of the FEM approximation is dictated by the discretization of the heart/volume projection (A_{IH}) and the volume conductor (the left-side matrix).

Inadequacy of Uniform Refinement. Most adaptive refinements designed for forward problems are essentially equivalent to uniform refinement if not considering cost and efficiency. Although uniform refinement indeed improves the three approximation issues aforementioned, it worsens the conditioning property of K. Fig 1 compares the forward solution error and the singular values of K resulting from uniformly refining a 2D torso mesh. Singular value decomposition is an effective means for evaluating the numerical quality of K, because it reveals how each spatial-frequency component of u_H contributes to u_T[2]. A well-conditioned system is characterized by a slowly-descending singular value spectrum and a large proportion of nontrivial singular values. Fig 1 shows while uniform refinement reduces the forward solution error, it extends the number of trivial singular values of K, thereby lowering the proportion of the recoverable components of u_H, which are associated with non-trivial singular values. This is because the ill-conditioning of K is an exponential function of the spatial frequency determined by the fidelity of epicardium[3]. Practitioners should assess this fidelity

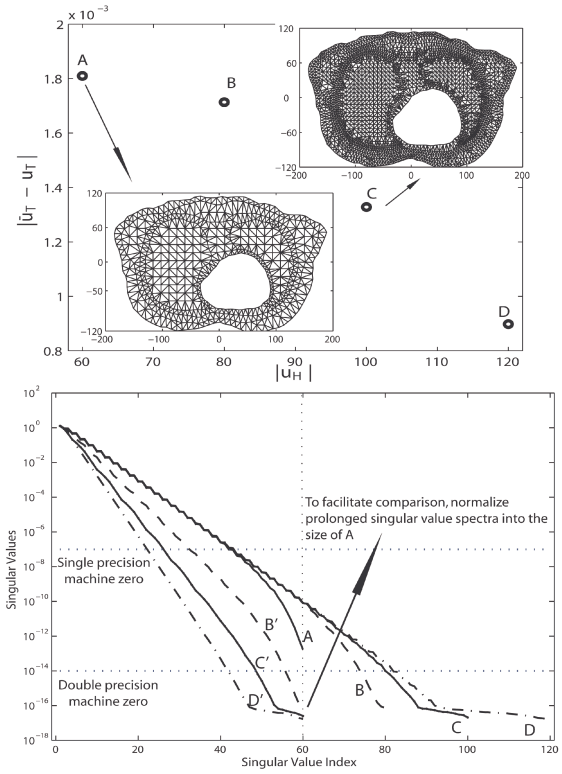

Figure 1. Top: forward solution error from four increasingly refined meshes labeled as A-D. Mesh A and C are displayed. $|u_H|$ is the epicardial resolution. $|\bar{u}_T - u_T|$ is the forward solution error. Bottom: singular value spectra of $\mathbf{K}$. Curves A-D are singular values in their original length; Curves B-D are normalized to the length of A, shown as B'-D'.

based on satisfying the clinical needs, but be cautious to solve beyond the limit.

The guidelines for discretizing the inverse ECG problem should be stated as follows: 1)determine a reasonable resolution on epicardium and 2)refine the volume and heart/volume projection while fixing the heart boundary. Such requirement leads to our advocacy of hybrid-shaped FEM and linear truncation from high-order finite elements.

Hybrid Finite Elements. The two guidelines pose a technical challenge to triangular or tetrahedral elements, which are typically available in commodity mesh generators, because such requirement leads to ill-shaped elements that by themselves cause extra numerical problems. We place quadrilateral elements (2D) and prismatic elements (3D) around the epicardium, as illustrated by Fig 2. The quads/prisms can be refined along their normal direction to capture the high potential gradient near the heart, without affecting the resolution on the epicardium. Hybrid elements is simple to implement: we first built quads/prisms from the triangulated bounding surfaces before calling tetrahedral mesh-generating routines. This paper will present some results in 3D. We refer to [3] for

detailed investigation of hybrid elements in 2D.

Linear Truncation from High-Order Elements. The finite element community has long been approximating continuous equations with high-order basis polynomials, which achieve higher accuracy and faster convergence rate than linear finite elements. High-order interpolation in an element can be made hierarchical, composed by linear, quadratic, cubic basis functions, *etc.* The coefficients of linear components have a physical meaning of being the voltage value on the nodes of the element, whereas all high-order components are made zero on mesh nodes. It can be seen that a high-order FEM is built from a linear FEM, but adding approximation by higher-order polynomials. Accordingly, (9) can be rewritten as follows (for simplicity, we present a quadratic expansion here):

$$\begin{pmatrix} \boldsymbol{u}_T^1 \\ \boldsymbol{u}_T^2 \end{pmatrix} = \begin{pmatrix} K_{T,H}^{1,1} & K_{T,H}^{1,2} \\ K_{T,H}^{2,1} & K_{T,H}^{2,2} \end{pmatrix} \begin{pmatrix} \boldsymbol{u}_H^1 \\ \boldsymbol{u}_H^2 \end{pmatrix} \tag{10}$$

where the superscript indicates the order of each component of $\boldsymbol{u}_T$ or $\boldsymbol{u}_H$. Our truncation scheme solves only the linear part of this high-order expansion:

$$\boldsymbol{u}_T^1 = K_{T,H}^{1,1} \boldsymbol{u}_H^1. \tag{11}$$

Such truncation is based on two concerns: (1) to preserve the pre-determined epicardium resolution, (2) $\boldsymbol{u}_T$ is piecewise linear because measurements are made only on mesh nodes. Note that (11) differs from (9) in that it contains high-order expansion of A_{II} and A_{IH} given in (8).

This truncation scheme provides a seamless approach of refining the heart/torso projection and the volume conductor (by high-order FEM) while preserving the epicardial resolution (by truncation). As the truncation is conducted in a hierarchical polynomial space, it keeps the smoothness of the solution and avoids aspect-ratio problems that obstruct spatial refinement methods. We found third-order FEM was sufficient for the inverse ECG problem.

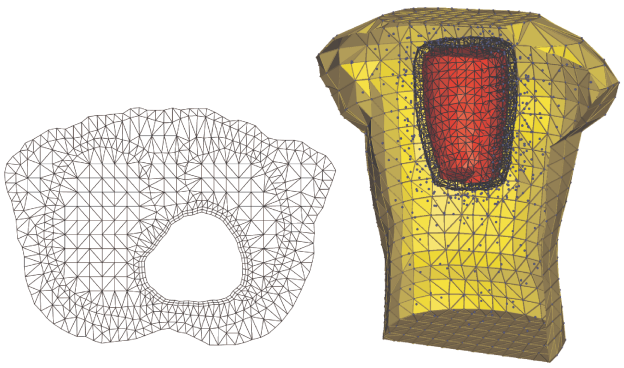

Figure 2. (Left): a segmented 2D torso slice with two layers of quadrilaterals around the heart. (Right): the torso/cage geometry with one layer of prisms around the cage. The rest torso volume is filled by tetrahedra. For simplicity, volume mesh is not shown completely. The dark dots represent vertices of the tetrahedral volume mesh.

Regularization Method. We solve the inverse problem (9) or (11) by the Tikhonov method given as follows:

$$\boldsymbol{u}_H(\lambda) = argmin \left\{ \|\mathbf{K}\boldsymbol{u}_H - \boldsymbol{u}_T\|^2 + \lambda^2 (\|\boldsymbol{u}_H\|^2 + \alpha^2 \|\nabla \boldsymbol{u}_H\|^2) \right\}$$

where λ and α are determined by exhaustive search. Our goal is to compare inverse solutions resulting from various refinements under an identical regularization framework.

3. Results and discussion

Hybrid Finite Elements. We present a hybrid elements model consisting of an isotropic torso tank and a canine heart surrounded by a cylinder cage on which potentials are measured. The model is illustrated by Fig 2. Using cage potentials rather than real epicardial potentials eliminates geometric variation incurred by heart contraction. The torso surface consists of 771 nodes and 1538 triangular elements whereas the cage has 602 nodes and 1200 triangles. This boundary discretization was kept intact during this test. We ran the forward simulation to obtain torso potentials, which, after being added with noise, served as the input for the inverse calculation. Fig 3 compares an ordinary tetrahedral mesh with a hybrid-element mesh having one layer of 10mm-thick prisms around the cage. The comparison is made in a coarse level and a refined level.

Fig 3 shows the hybrid mesh yields better singular values of $\mathbf{K}$ than the pure tetrahedral mesh under both discretization levels. The hybrid mesh achieves this numerical superiority with less elements, implying its advantage in efficiency. It holds for both mesh types that refining volume while keeping boundary resolutions extends nontrivial singular values of $\mathbf{K}$. In the tetrahedral meshes or hybrid meshes, the gap between the singular value spectrum of the coarse mesh and that of the refined mesh indicates the increased ill-conditioning caused by insufficient discretization but not associated with ill-posedness of the continuum problem. Any finite element discretization should consciously avoid such numerically-induced ill-conditioning. Fig 3 (bottom) shows the cage potentials calculated at the instant when it had the largest spatial variances (thus the most difficult to recover). The activation wavefront is captured well. Hybrid meshes outperform pure tetrahedral meshes in recovering the magnitude of local extrema. Volume refinement leads to better recovery of the secondary local extrema (Panel C and D).

Linear Truncation from High-Order FEM. Our truncation method was conducted on a 2D torso mesh analogous to the one shown in Fig 2 but without quadrilaterals. The mesh, segmented to conform to interfaces between various tissues, contains 1071 triangles, including 60 nodes on the epicardium and 105 nodes on the torso

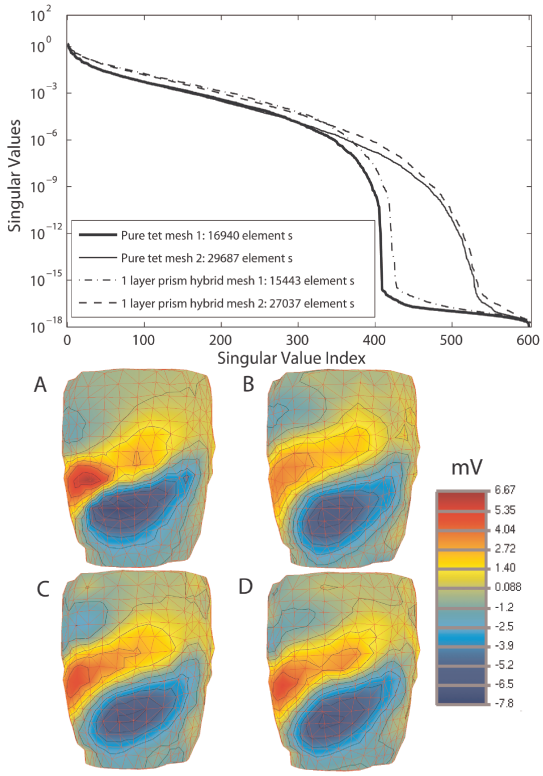

Figure 3. Top: singular values of $\mathbf{K}$ resulting from pure tetrehedral meshes and hybrid meshes with one layer of prisms around the cage. Each mesh type includes two meshes with identical boundary discretization but different volume discretizations. Bottom: cage potentials calculated under 1% input noise. (A) exact values; (B) potentials computed from pure tetrahedral mesh with 16940 elements; (C) potentials computed from hybrid mesh with coarse volume (15443 elements); and (D) potentials computed from hybrid mesh with refined volume (27037 elements).

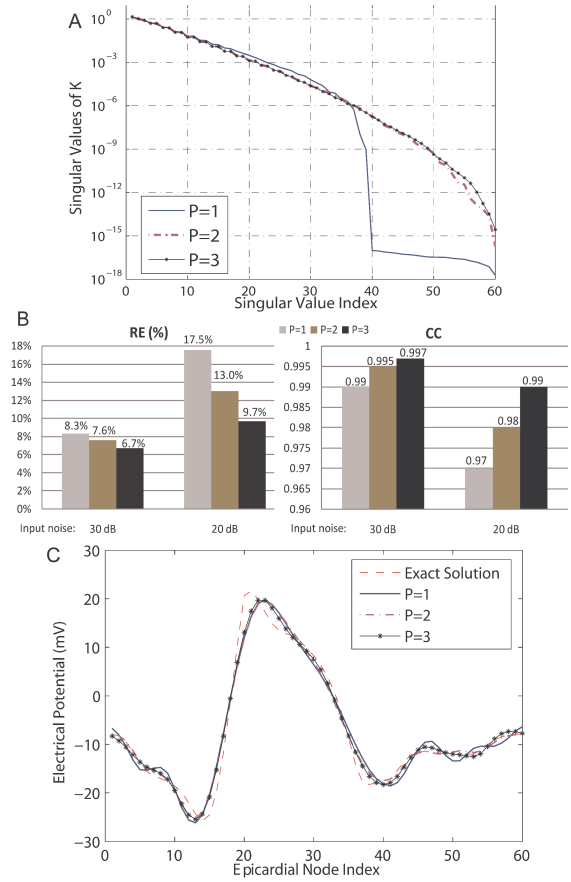

Figure 4. Linear truncation from first-, second- and third-order finite elements, marked by $P = 1, 2, 3$. (A) singular values of the respective resulting $\mathbf{K}$; (B) relative error (RE) and correlation coefficient (CC) of the inverse solution calculated under two levels of input noise; (C) reconstructed epicardial potentials under 20dB input noise.

surface. We tested isoparametric finite elements of first-, second-, and third-order, and the results are summarized in Fig 4. Fig 4(A) shows high-order refinement consistently improves the singular values of $\mathbf{K}$, a similar effect to spatial refinement of the volume. The convergence of singular values from the second-order FEM to the third-order FEM implies the discretized problem has reached the same quality as the original continuous problem. In other words, refinement "saturates" to its asymptotic performance.

Fig 4(B) assesses the inverse solution by its relative error (the ratio of the error to the exact solution, in Euclidean norm) and its correlation coefficient with the exact solution. The inverse solution was calculated with zero-mean Gaussian noise of 30dB and 20dB being added to the torso measurements. With the truncation method, high-order refinements effectively reduce the error and improve the correlation coefficient. Fig 4(C) displays an example of recovered epicardial potentials under 20dB noise. The linear truncation from third-order FEM yields the best solution.

4. Conclusions

We studied the FEM discretization for the inverse problem and proposed hybrid-shaped elements and truncating linear parts from high-order elements. Both methods alleviate the ill-conditioning and improve the inverse solution.

References

[1] Johnson CR. Adaptive finite element and local regularization methods for the inverse ecg problem. In Inverse Problems in Electrocardiology. WIT Press; 2001.

[2] Messnarz B, Seger M, *et al.* A comparison of noninvasive reconstruction of epicardial versus transmembrane potentials in consideration of the null space. IEEE Trans BME 2004; 51(9):1609–18.

[3] Wang D, Kirby RM, Johnson CR. Resolution strategies for the finite element based solution of the electrocardiograph inverse problem. accepted by IEEE Trans BME ;2009.